Supporting information

Modelling post-plasma quenching nozzles for improving the performance of CO_2 microwave plasmas

Senne Van Alphen[1,2], Ante Hecimovic[3], Christian K. Kiefer[3], Ursel Fantz[3], Rony Snyders[2], Annemie Bogaerts[1]

[1] Research group PLASMANT, University of Antwerp, Belgium

[2]Research group ChIPS,University of Mons, Belgium

[3] Max-Planck-Institut für Plasmaphysik, Germany

S.1 The finite element mesh

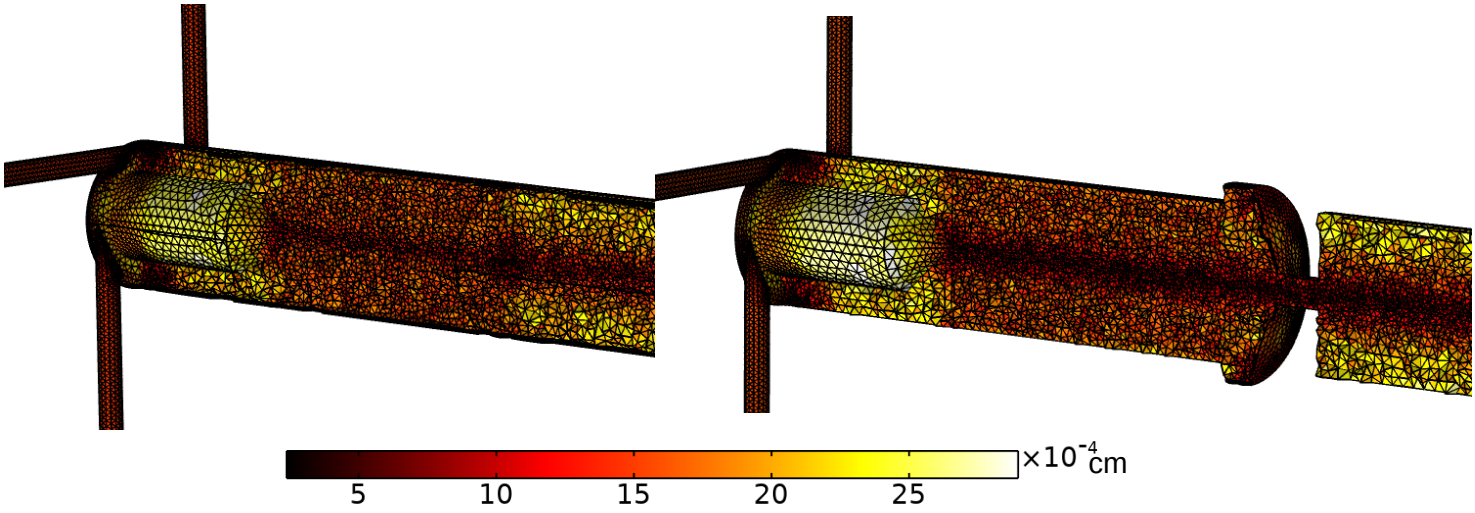

Figure S1: Finite element mesh of the simulation domain of the MW reactor geometry a) without nozzle attached and b) with nozzle attached. The color scale indicates the size of the mesh elements.

Figure S1 presents the finite element mesh of the 3D CFD model domain, in which the color scale indicates the size of the mesh elements. The simulation domain consists of 700 000 tetrahedral-shaped mesh elements, in which the size of the elements is reduced specifically in zones where physical properties are expected to display high gradients, e.g. in the center of the reactor where the plasma filament is located, in the throat of the nozzle, in the inlet tubes. To resolve the thin boundary layers of the fluid along the no-slip boundaries (i.e. u = 0 m/s) of the reactor walls , the finite element mesh near the walls consists of 4 mesh boundary layers with dense element distribution in the normal direction along the walls of the reactors.

This mesh was refined by re-solving the model on progressively finer meshes until the solution remained mesh independent. In this form, the models take 6-10h to solve (without parallelization) on a desktop equipped with an Intel Core i7-5820K CPU and 64.0 GB RAM, using a relative tolerance of 0.001 as conversion criterium.

S.2 The turbulent gas flow

We apply the Menter's Shear Stress Transport (SST) model,[1] which uses the common k-ε model in the free stream and combines it with the more accurate k-ω model near the walls, where the flow is more complicated.

This approach includes the following equations for the turbulent kinetic energy k and the specific dissipation ω:

$$\rho_g(\overrightarrow{u_g}.\nabla)k = \nabla\cdot[(\mu+\mu_T\sigma_k)\nabla k] + P - \beta_0\rho_g\omega k \qquad (S.1)$$

$$\rho_g(\overrightarrow{u_g}.\nabla)\omega = \nabla\cdot[(\mu+\mu_T\sigma_\omega)\nabla\omega] + \frac{\gamma}{\mu_T}\rho_g P - \beta_0\rho_g\omega^2 + 2(1-f_{v1})\frac{\sigma_{\omega2}\rho_g}{\omega}\nabla k\cdot\nabla\omega \qquad (S.2)$$

Where ρ_g stands for the gas density, $\overrightarrow{u_g}$ is the gas flow velocity vector, μ is the dynamic viscosity, σ_k, σ_ω and γ are model coefficients defined in equations S.10, S.11 and S.12 below, and β_0 and $\sigma_{\omega2}$ are dimensionless model constants defined in table S1. The other symbols are explained below.

In equations S.1 and S.2, μ_T is the turbulent viscosity of the fluid and is defined as:

$$\mu_T = \frac{a_1 k}{max(a_1\omega, Sf_{v2})} \qquad (S.3)$$

In which S is the absolute strain rate and a_1 is a dimensionless model constant, defined in table S1. In equations S.2 and S.3, f_{v1} and f_{v2} are two blending functions that control the switch from the k-ω model to the k-ε model in the free stream (where f_{v1} = 1)

$$f_{v1} = \tanh\left(\min\left(\theta_2^2, \frac{4\sigma_{\omega2}k}{CD_{k\omega}y^2}\right)\right)^4 \qquad (S.4)$$

$$f_{v2} = \tanh(\theta_2^2) \qquad (S.5)$$

In which y is the y-component of the position vector, and θ_2 and $CD_{k\omega}$ are placeholders for the following terms:

$$CD_{k\omega} = max\left(2\rho\sigma_{\omega2}\frac{1}{\omega}\frac{\partial k}{\partial x}\frac{\partial\omega}{\partial x},\ 10^{-10}\right) \qquad (S.6)$$

$$\theta_2 = max\left(\frac{2\sqrt{k}}{\beta_0\omega l_W^2}, \frac{500\mu}{y^2\omega}\right) \qquad (S.7)$$

In which l_W is the wall distance.

In equations S.1 and S.2, P serves as a product limiter coefficient and is defined as:

$$P = \min(P_k 10\rho\beta_0 k\omega) \quad (S.8)$$

In which P_k is a placeholder for the following term:

$$P_k = \mu_T \left(\nabla\overrightarrow{u_g} \cdot \left(\nabla\overrightarrow{u_g} + \left(\nabla\overrightarrow{u_g}\right)^T\right) - \frac{2}{3} \cdot \left(\nabla \cdot \overrightarrow{u_g}\right)^2\right) - \frac{2}{3}\rho k \nabla \cdot \overrightarrow{u_g} \quad (S.9)$$

The model coefficients in equations S.1 and S.2 are defined as:

$$\sigma_k = f_{v1} \cdot \sigma_{k1} + (1 - f_{v1})\sigma_{k2} \quad (S.10)$$

$$\sigma_\omega = f_{v1} \cdot \sigma_{\omega 1} + (1 - f_{v1})\sigma_{\omega 2} \quad (S.11)$$

$$\gamma = f_{v1} \cdot \gamma_1 + (1 - f_{v1})\gamma_2 \quad (S.12)$$

In which σ_{k1}, σ_{k2}, $\sigma_{\omega 1}$,$\sigma_{\omega 2}$, γ_1 and γ_2 are dimensionless model constants, defined in table S1.

Table S1: Dimensionless model constants used in the SST turbulent flow model.

σ_{k1}	0.85
σ_{k2}	1
$\sigma_{\omega 1}$	0.5
$\sigma_{\omega 2}$	0.856
γ_1	0.5556
γ_2	0.44
a_1	0.31
β_0	0.09

S.3 Gas flow velocity profiles of the quasi-1D chemical kinetics model

Using the axial gas flow velocity calculated by the 3D CFD model, we can convert the time dependence of a 0D chemical kinetics model to a spatial dependence over a straight line in the reactor, resulting in a quasi-1D model. The axial gas flow velocity profiles in the center of the reactor, which are used in this conversion, are presented for two different flow rates in figure S2, for a) a reactor without and b) a reactor with 5 mm nozzle attached. The figures clearly display the increase in gas flow velocity as the gas flows through the narrow nozzle gap.

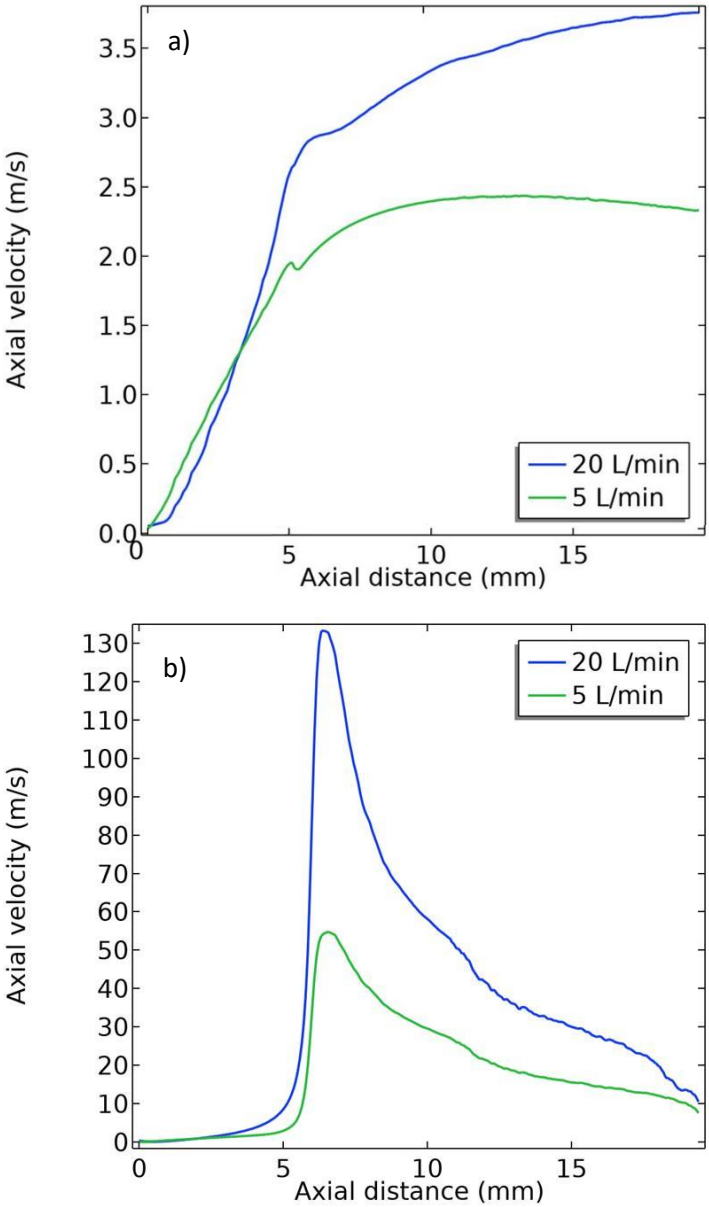

Figure S2: Axial velocity profile in the center of the reactor as calculated by the 3D CFD model for a reactor a) without and b) with 5 mm nozzle attached.

S.4 Boundary conditions in the model

For the calculation of the gas flow velocity field $\vec{u}$ (u,v,w) and pressure p inside the reactor, the following boundary conditions are introduced in the model geometry when solving the Navier-Stokes equations (equations 1 and 2 of the main paper):

At the Inlet:

$$\vec{u} = \vec{u}_0 \tag{S.13}$$

In which $\vec{u}_0$ is the flow velocity defined by the input flow rate.

$$k = \frac{3}{2}(u_0 I_T)^2 \tag{S.14}$$

$$\omega = \frac{k^{\frac{1}{2}}}{(\beta_0)^{\frac{1}{4}} L_T} \tag{S.15}$$

Where u_0 is the input flow rate, I_T the expected turbulence intensity (here 0.05 for medium intensity), β_0 a dimensionless model constants shown in table S1 and L_T the turbulence length scale.

At the reactor walls:

$$\vec{u} = 0 \tag{S.16}$$

Where the velocity is zero as a result of the "no slip" condition at the walls.

At the outlet:

$$\left[-p\vec{I} + \mu(\nabla\vec{u} + \nabla(\vec{u})^T) - \frac{2}{3}\mu(\nabla \cdot \vec{u})\vec{I}\right]\vec{n} = p_0\vec{n}_{outlet} \tag{S.17}$$

In which p_0 is the pressure at the outlet, and $\vec{n}_{outlet}$ the unit vector normal to the outlet boundary.

For the calculation of the gas temperature T_g, the following boundary conditions are introduced in the model geometry when solving the heat balance equation (equation 3 of the main paper):

At the Inlet:

$$-\vec{n}_{inlet} \cdot \vec{q} = \rho\vec{u}\int_{T_{inlet}}^{T} C_p dT_g \cdot \vec{n}_{inlet} \tag{S.18}$$

In which T_{inlet} is the gas temperature of the inlet stream, usually 293.15 K, and $\vec{n}_{inlet}$ the unit vector normal to the inlet boundary.

At the reactor walls:

For the heat loss through the reactor walls to the environment at a heat loss rate q_{loss}, the boundary condition states:

$$-\vec{n}_{wall} \cdot \vec{q} = q_{loss} \tag{S.19}$$

$$q_{loss} = h(T_{ext} - T_g) \qquad (S.20)$$

In which $\vec{n}_{wall}$ is the unit vector normal to the wall boundary, T_{ext} is the gas temperature of the environment, usually 293.15 K and h the heat transfer coefficient of the reactor wall material (10 W/(m²*K) for the quartz tube).

At the outlet:

$$-\vec{n}_{outlet} \cdot \vec{q} = 0 \qquad (S.21)$$

In which $\vec{n}_{outlet}$ is the unit vector normal to the wall boundary.

S.5 The thermodynamic and transport properties of the model

All thermodynamic and transport properties of the gas, i.e. the viscosity, the thermal conductivity and the heat capacity are adopted from Magin et al.[2], where these properties are calculated for a wide range of temperatures assuming thermodynamic equilibrium. This means that changes in gas composition and energy balance due to chemical reactions are taken into account within these properties, e.g. the endothermic characteristic of CO_2 splitting, as well as the formation of CO and O_2 and the destruction of CO_2 are represented in the heat capacity and thermal conductivity. However, as these properties are calculated assuming thermodynamic equilibrium, the properties assume that chemical equilibrium is reached very fast as the temperature increases or decreases. This assumption is reasonable in an atmospheric MW plasma torch, because at 6000 K, which is the core temperature of the plasma filament, chemical equilibrium is reached within milliseconds, which is very fast compared to the timescale of the residence time in the reactor (in the seconds range). In the effluent of the reactor, however, chemical equilibrium is reached slower, so the impact of chemistry on the heat balance is not completely accounted for in this part of the reactor. However, at this point the heat balance is mostly defined by the hot gas flowing form the 6000 K plasma zone, rather than recombination reactions heating the gas, which makes the error of the assumption relatively small.

S.6 Representing the plasma as a heat source

By representing the plasma as a heat source using the thermal balance equation (equation 3 in the main paper), the 3D shape of the plasma is required as input for the model.

This heat source term (Q) is then defined as:

$$Q = N * rad(x) * rad(y) * ax(z)$$

In which rad and ax are the radial and axial power profiles of the MW power, respectively, and N is a normalization factor, such that:

$$\iiint Q\, dx\, dy\, dz = P_{MW}$$

Where P_{MW} is the microwave power that is absorbed by the plasma, measured in the experiments. The radial and axial power profiles (rad and ax) are defined using analytical functions that approximate the radial and axial profile of a contracted plasma filament, as measured by D'Isa et al.[3] and Wolf et al.[4]. The radial power profile used in the model, is shown in figure S3a, resembling closely the profile measured by D'Isa et al., shown in figure S3b. The axial power profile used in the model, is shown in figure S4a, resembling closely the profile measured by D'Isa et al., shown in figure S4b. Furthermore, as concluded in the work from D'Isa et al., the plasma diameter and length of the plasma is independent on the flow,[3] allowing us to use the same power profile for every flow rate.

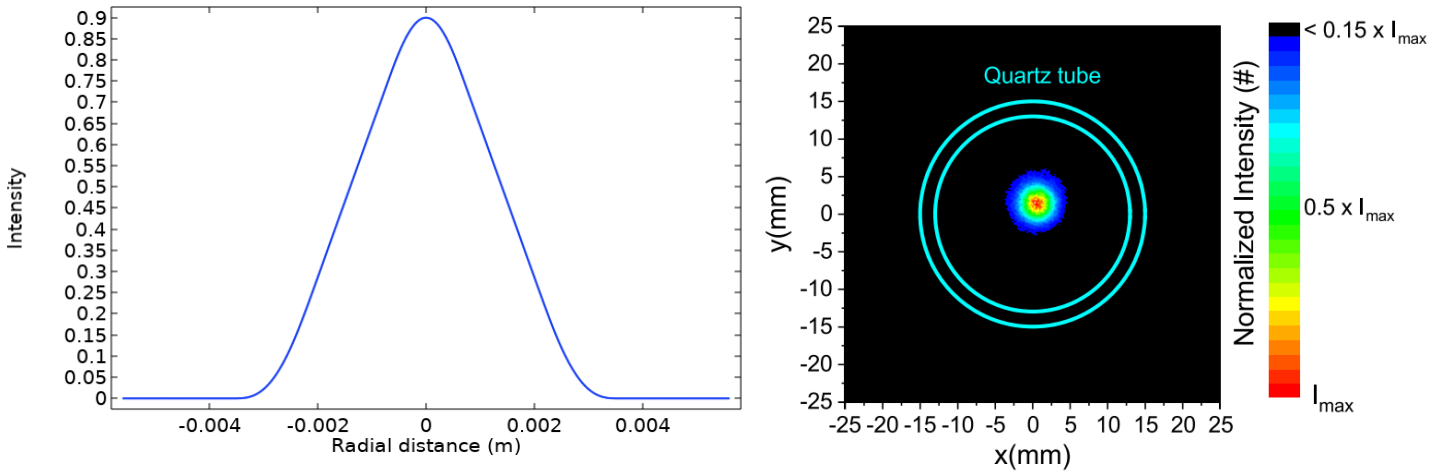

Figure S3: a) Radial power density profile of the plasma assumed in the model
b) Radial ICCD image taken by D'Isa et al

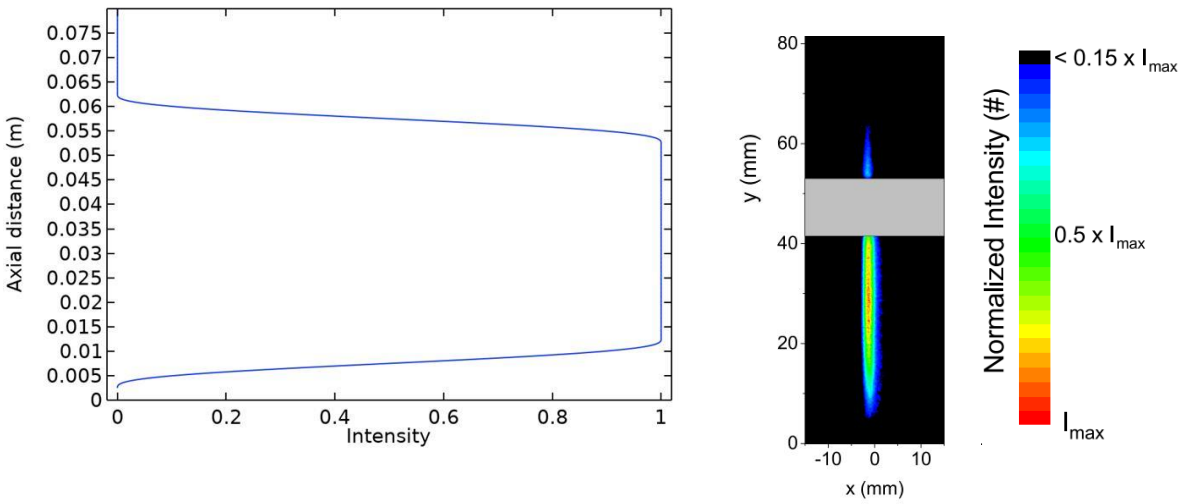

Figure S4: a) Axial power density profile of the plasma assumed in the model
b) Axial ICCD image taken by D'Isa et al.

References

(1) Menter, F. R.; Kuntz, M.; Langtry, R. Ten Years of Industrial Experience with the SST Turbulence Model Turbulence Heat and Mass Transfer. *Turbul. Heat Mass Transf.* **2003**, *4*, 625–632.

(2) Magin, T.; Degrez, G.; Sokolova, I. Thermodynamic and Transport Properties of Martian Atmosphere for Space Entry Application. *33rd Plasmadynamics Lasers Conf.* **2002**, No. May.

(3) D'Isa, F. A.; Carbone, E. A. D.; Hecimovic, A.; Fantz, U. Performance Analysis of a 2.45 GHz Microwave Plasma Torch for CO2. *Plasma Sources Sci. Technol.* **2020**, *29*.

(4) Wolf, A. .; Righart, T. W.; Peeters, F. J.; Bongers, W. .; van de Sanden, M. C. Implications of Thermo-Chemical Instability on the Contracted Modes in CO2 Microwave Plasmas. *Plasma Sources Sci. Technol.* **2020**, *29*, 025005.